Journal of Visualization, Vol. 1, No. 1 (1998) 37-50

Infrared Thermography as a Tool for Thermal Surface Flow Visualization

Carlomagno, G. M.*, Cardone, G.*, Meola, C.*, and Astarita, T.*

* Università degli Studi di Napoli "Federico II", Dipartimento di Energetica, Termofluidodinamica Applicata e Condizionamenti Ambientali (D.E.T.E.C.), P.le Tecchio 80, 80125 Napoli, Italy.

Received 23 July 1997.
Revised 16 November 1997.

***Abstract*:** Infrared (IR) thermography is a two-dimensional, non-contact technique of temperature measurement which can be usefully exploited in a vast variety of heat transfer industrial applications as well as research fields. The present work focuses attention on thermal surface flow visualizations of several types of fluid flow studied by means of the IR imaging system and in particular: the flow over a delta wing at angle of attack; the flow generated by a disk rotating in still air; air jets impinging on a flat wall; the flow inside a 180deg turn in a *static* channel with, or without, turbulence promoters; the flow inside a 180deg turn in a *rotating* square channel. Each flow visualization is illustrated through thermographic images and/or Nusselt number maps. The emphasis is on the capability of the infrared system to study: laminar-to-turbulent transition and location of primary and secondary vortices over the delta wing at angle of attack; the spiral vortical structure developing at transition over the disk; azimuthal structures arising for certain jet conditions; the influence of the channel aspect ratio (width to height ratio) on the heat transfer coefficient distribution along the 180deg turn, as well as the influence of ribs, in the case of *static* channel; the influence of rotation for the rotating channel.

***Keywords*:** flow visualization, infrared thermography, convective heat transfer.

Nomenclature:

AR	channel aspect ratio
Bi	Biot number, hb/λ
b	thickness of the foil
Bu	buoyancy parameter, $\beta(T_w-T_b)$
c	root chord of the delta wing
c_p	specific heat at constant pressure
D	nozzle diameter
d	hydraulic diameter
h	convective heat transfer coefficient
k	thermal conductivity of air
M	Mach number
Nu	Nusselt number, hd/k
q	heat flux
R	local radius
Re	Reynolds number, Vc/ν
Re_d	Reynolds number, Vd/ν
Re_ω	Reynolds number, $\omega\Delta^2/\nu$
Ro	rotation number, $\omega d/V$
s	local wing semispan

St Stanton number, $St = h/(\rho c_p V_\infty)$
T temperature
V velocity
Z impingement distance

Greek symbols

α angle of attack
β thermal expansion coefficient of air
Δ disk diameter
ε total emissivity coefficient
ε_λ spectral emissivity coefficient
γ rib inclination angle
λ thermal conductivity of the foil
ν kinematic viscosity of air
ρ density of air
σ Stefan-Boltzmann constant
ω angular speed

Subscripts

a ambient
aw adiabatic wall
b bulk
c lateral conduction
l losses
o stagnation
r radiative
R reference
w wall
∞ free stream

Superscripts

* as per Dittus-Boelter equation

1. Introduction

Infrared thermography is a measurement technique of surface thermal maps. The infrared scanning radiometer (IRSR) consists basically of a camera which detects the electromagnetic energy radiated in an infrared spectral band by an object (whose surface temperature distribution is to be measured) and converts it into an electronic video signal.

The IRSR can be regarded as a true two-dimensional temperature sensor since it allows accurate measurements of surface temperature maps also in presence of high spatial temperature, and/or heat-flux, gradients; its spatial resolution mainly depends on the camera and on the employed optics. The IR system generally measures the object skin temperatures and so it can also be regarded as a thin-film sensor or, better, as a two-dimensional array of thin films; however, the response time of IRSR is typically of the order of 10^{-1}–10^{-2} s.

IR thermography can be fruitfully employed to perform thermal surface flow visualizations as well as to measure convective heat fluxes either in steady, or in transient, techniques. In both cases, the pertinent heat transfer equation applied to the specific sensor model yields the relationship by which the map of the measured temperatures is correlated to the corresponding distribution of the heat transfer rate.

If compared to standard sensors, the use of IRSR as a temperature sensor in convective heat transfer measurements appears advantageous from several points of view; IRSR is a fully two-dimensional sensor and is non-invasive, i.e., it does not involve conductive errors which exist through the wires of thermocouples or thermistors. The accuracy of the measurement depends mainly on the knowledge of the emissivity coefficient of the surface viewed by the IR camera; however, an error in the evaluation of the emissivity coefficient generally leads to a smaller error in the temperature measurement.

As illustrated by Carlomagno (1993) the use of a fully computerized infrared imaging system matches both

qualitative and quantitative requirements. In certain applications, as in shock tunnels (Simeonides et al., 1989; Henckels et al., 1990), or when dealing with moving objects (Cardone et al., 1996), the so-called *line-scan* option (consisting of locking the *vertical* scanning mechanism of the radiometer) may be used to respectively decrease the response time, or to reconstruct the thermal image. Of course, unless the object is moving, in the *line-scan* mode the measurement is intrinsically one-dimensional.

In the case of an iposonic flow regime ($M<<1$), the aerodynamic heating is not adequate for the IRSR sensitivity, so it is necessary to create a temperature difference between the model surface and the flow, i.e. it is necessary to transfer heat to the model in the so-called *active* mode.

Models of cylindrical geometry (e.g. 2D airfoils, pipes, plates etc.) can be easily heated by Joule effect by making their surface of a very thin metallic foil, or of a thin printed circuit board. In these cases, the convective heat transfer coefficient from the model surface to the flowing stream is measured by the so-called *heated-thin-foil* technique. By applying this technique Carlomagno and co-workers study several fluid flow configurations which are of industrial and academic interest. In most cases IR thermography turns out to be an indispensable quick mean to deal with complex fluid dynamic situations since it allows observation of some particular phenomena; amongst others the laminar-to-turbulent transition, the location and extension of separation bubbles and reattached regions as well as the formation of azimuthal structures and vortices.

De Luca et al. (1990) characterize the boundary layer development over a wing model to detect transition and separation regions; they relate the measured convective heat transfer data to the wall skin friction by means of the Reynolds analogy. The beginning and the extension of the laminar region, the location of turbulent reattachment points, as well as the regions where the turbulent boundary layer is separated, are quickly identified all over the leeside surface of the tested wing model even for the case of highly three-dimensional flow.

Carlomagno (1996) performs surface flow visualizations and heat transfer measurements in a backward-facing step flow. In the specific case, the use of the radiometer is found to be particularly advantageous to follow the flow displacement downstream of the step, as the Reynolds number varies from very low values up to 50 000.

At high Mach numbers, because of the stream high kinetic energy content, the detection of the thermal image may be obtained by the so-called *passive* mode. Generally, the model, initially at uniform ambient temperature, is suddenly exposed to the high total temperature air stream; according to the properly selected thermal model, the *thin-skin* (e.g. Carlomagno, et al., 1991) or the *thin-film* (e.g. Bynum et al., 1976; de Luca et al., 1992) techniques are used to obtain the convective heat transfer coefficients and/or to investigate the boundary layer behavior.

Anyhow, it has to be pointed out that accurate temperature measurements by means of thermography can be performed on condition that all the potential error sources linked to the object, the environment and the acquisition system can be eliminated. In fact, a correct use of infrared thermography involves: characterization of the IR imaging system performance, calibration of the camera, use of additional external optics and/or magnifying mirrors to improve the spatial resolution, determination of the surface emissivity, correct identification of the measured points, design of the optical access window within the choice of the most appropriate IR material. A discussion about these general aspects is reported by Carlomagno and de Luca (1989) and Balageas et al. (1991).

In the present work attention is focused on some thermal surface flow visualizations obtained by means of infrared thermography and performed with the *heated-thin-foil* technique. The capability of IR thermography to characterize the thermal behavior of the flow in several fluid configurations is highlighted; in particular, the flow over a delta wing at angle of attack; the flow instability generated at transition by a disk rotating in still air; air jets impinging on a flat wall; the flow inside a 180 deg turn in a static channel with, or without, ribs; the flow inside a 180deg turn in a *rotating* square channel.

2. Steady-state Heated-thin-foil Technique

The *heated-thin-foil* method consists of heating a thin metallic foil by Joule effect and computing the convective heat transfer coefficient h from the foil to the stream flowing on it, by means of the relationship:

$$h = \frac{\dot{q} - \dot{q}_l}{T_w - T_R} \tag{1}$$

where: q is the known Joule heating; q_l includes the thermal losses mainly due to tangential conduction q_c and radiation q_r, T_w is the wall temperature which is measured when heating the foil (hot image) and T_R is a reference temperature. In the present case, the latter can be either the adiabatic wall temperature (which, for external flows,

corresponds to the cold image obtained without heating), or the bulk temperature of the stream for internal flows. The foil is generally thermally insulated at its backface, i.e. the face opposite to that the stream is flowing over. When this insulation cannot be accomplished, e.g. for optical access reasons, additional thermal losses, such as natural convection and radiation, must be taken into account. Generally, the measurement can be performed on both sides of the foil; in fact, if the Biot number $Bi = hb/\lambda$ (where λ and b are the foil thermal conductivity and thickness respectively) is relatively small, the foil can be considered isothermal across its thickness.

The tangential conduction q_c, which modulates the thermal signal, may be evaluated by means of the second derivative of the wall temperature T_w. The evaluation of the second derivative of T_w is eased by the fact that IRSR yields a very large number of wall temperatures. However, it has to be pointed out that spurious effects linked to the noise have to be avoided by filtering the temperature signal; in the steady state *heated-thin-foil* technique, the noise can be also strongly reduced by averaging a large number of thermal images acquired in a time sequence. When the *heated-thin-foil* is made of a printed circuit board, the bulk tangential thermal behavior of the foil may be non isotropic.

The losses due to radiation q_r may be evaluated according to the Stefan-Boltzmann law :

$$\dot{q}_r = \varepsilon\sigma(T_w^4 - T_a^4) \tag{2}$$

where ε is the total emissivity coefficient, σ is the Stefan-Boltzman constant and T_a is the ambient temperature. Under the assumption that the spectral emissivity coefficient ε_λ does not vary much, the total emissivity coefficient ε of the surface under test may be measured by the IR termography itself by relating the detected radiation from a specimen heated by means of a bath/circulator with its actual temperature monitored by a precise thermometer.

The infrared radiation measured by an IR system can also be affected by atmospheric damping and reflected radiation from object surroundings; these factors may be taken into account by calibration and correction procedures.

Mainly due to the finite dimensions of the IR temperature sensor, another modulation is introduced by the *Modulation Transfer Function* (*MTF*) of the camera that produces a signal of decreasing amplitude for increasing the spatial frequency. Moreover, when sampling the analog signal in single detector cameras, a further decrease of the temperature amplitude may be introduced by the analog-to-digital (A/D) converter, which leads to a *Sampling Modulation Response.*

All the aforementioned effects may reduce, to a greater or a lower extent, the temperature amplitude according to the experimental conditions, as well as to the measuring device, and evidence the need of restoration of the thermal image. This problem is addressed by Carlomagno (1997).

3. Applications

In the following, several different fluid flow configurations are analyzed by means of infrared thermography. For all the experiments the convective heat transfer coefficient h is evaluated by means of the *heated-thin-foil* technique, see Eq. (1). Of course, the measurement of T_w and T_R involves all the considerations already made in the previous section. The surface viewed by IR camera is always coated with a thin film of black opaque paint whose emissivity factor ε is equal to 0.95 in the bandwidth of interest.

The infrared thermographic system mainly employed is the AGEMA Thermovision 900. The field of view (which depends on the optics focal length and on the viewing distance) is scanned by the Hg-Cd-Te detector in the 8-12 μm infrared window. Nominal sensitivity, expressed in terms of noise equivalent temperature difference, is 0.07°C when the scanned object is at ambient temperature. The scanner spatial resolution is 235 instantaneous fields of view per line at 50% slit response function. Each image is digitized in a frame of 136 × 272 pixels at 12 bit. An application software is used, for each thermal image, which generally involves: noise reduction by numerical filtering, computation of temperature, evaluation of radiation and tangential conduction losses and heat transfer correlation.

3.1. Delta Wing

Delta wings are extensively adopted for high-performance aircraft configuration design. The leeward flowfield is dominated by highly organized vortical flow structures created by the separation of the boundary layer at the leading edge. These vortices are considered by Lee and Ho (1990) and Nelson (1991) to be responsible of the remarkable increase of wing lift which is observed at high angle of attack subsonic flight.

The complex flow over the wing at angle of attack and null sideslip angle, is schematically shown in Fig.1. The crossflow velocity components, which increase with the angle of attack, affect the boundary layer behavior on the windward surface so that the attached flow is deflected towards the leading edge where separation occurs (primary separation lines S_1 and S'_1 in Fig. 1).

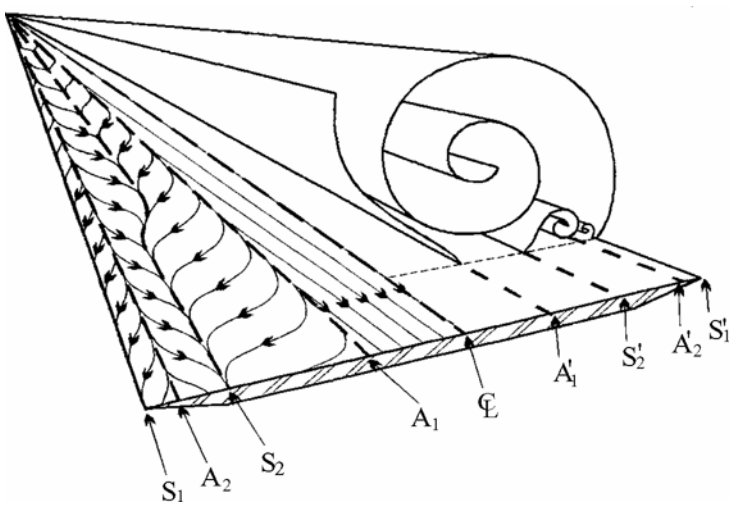

Fig. 1. Vortices on the leeward side of delta wing; *A*: reattachment lines; *S*: separation lines.

The separated shear layer is curved inboard over the upper wing surface where two symmetric stable counter-rotating vortical structures are generated. The flow is deflected symmetrically along curved streamlines and a forced reattachment is generated on the leeward wing surface in the vicinity of the root chord line ℄ (i.e. primary reattachment lines A_1 and A'_1). A second separation line S_2 exists underneath the primary vortex core; in fact, the boundary layer, after the primary reattachment, separates again giving rise to a couple of counter-rotating secondary vortices on each wing side which reattach on A_2 and A'_2.

The surface flow between the primary reattachment line A_1 and the secondary separation line S_2 is typically transitional; when transition occurs, the development of the boundary layer entails outward displacement of the secondary separation line S_2 whose location strongly depends on the Reynolds number and angle of attack.

The tested model is a 65° delta wing with sharp leading edge and with: root chord c = 850 mm, wing

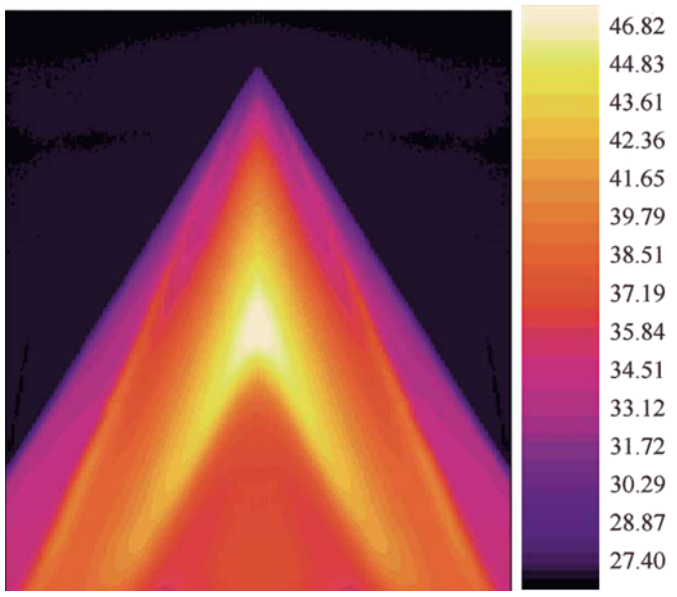

Fig. 2. Thermogram of the wing apex for $\alpha = 10^{\circ}$, $Re = 1.65 \times 10^6$.

semispan s = 396.4 mm, bevel angle 30° and wing thickness about 22 mm. Measurements are performed in steady conditions for Reynolds number (based on the root chord c) ranging from 1.10×10^6 to 2.19×10^6. The angle of attack α is varied from 6° to 30°. The convective heat transfer coefficient is calculated from Eq.(1) with $T_R = T_\infty$ and the radiative thermal losses are computed by means of Eq. (2); the conductive losses are neglected.

The temperature distribution in the tip region of the leeward wing surface is shown in the thermogram of Fig.2 for α = 10°, Re = 1.65×10^6, T_∞ = 27.5°C and the same distribution shifted towards the trailing edge is reported in the 3D map of Fig.3. It is worth noting that regions over the model (heated in wind conditions) which display higher temperature are characterized by lower heat transfer coefficients and *vice versa.*

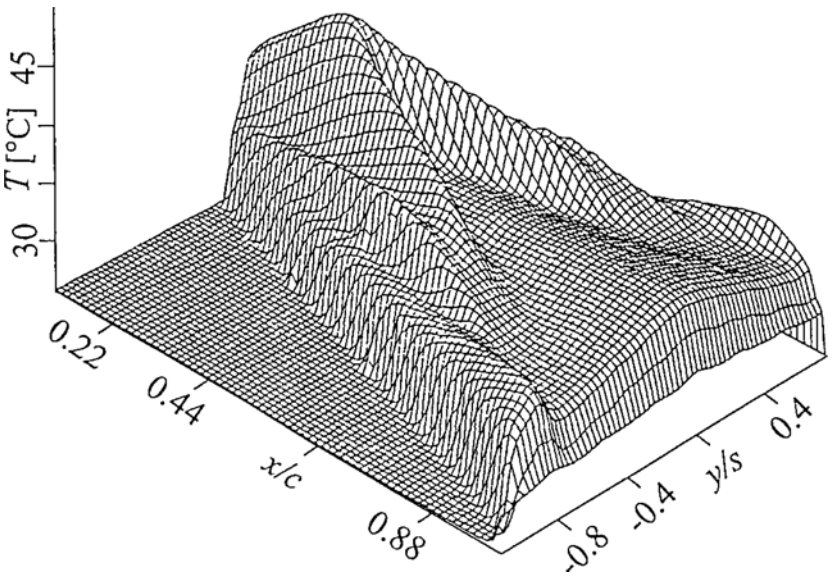

Fig. 3. Relief map for α = 10°, Re = 1.65×10^6.

From Figs.2 and 3 it is evident that the central region of the wing surface is characterized by an almost two-dimensional flow development; moving from the model apex in streamwise direction along the root chord, a gradual increase in temperature is firstly observed which is due to the growth of the laminar boundary-layer thickness that causes a reduction of the convective heat transfer coefficient. After laminar-to-turbulent transition, the heat transfer is intensified and, therefore, the temperature of the wing surface decreases; finally the thickening of the turbulent boundary layer produces another slighter positive temperature gradient.

Nearby the leading edge, a region of high temperature (low heat transfer coefficients due to the primary separation) should be present; this however does not occur because of the edge effects which are mainly due to the presence of the solid, not thermally insulated, bevel. Moving along the wing span in the laminar zone of the wing (i.e. nearby its apex), a temperature increase is firstly observed followed by a decrease and a successive increase. The locus of the side local temperature maximum lies over a straight line (originating from the wing apex) which represents the secondary separation line; the locus of the local minimum identifies the primary reattachment line. The secondary reattachment line is not completely visible because too close to the leading edge and therefore masked by the edge effects. The outboard displacement of the secondary separation line towards the leading edge is clearly evident after transition and is due to the higher stability of the turbulent surface flow; also the primary reattachment line moves towards the wing leading edge. It is worth noting that the Reynolds number influences transition; in more details, transition anticipates as Re increases, as a consequence the extension of the laminar region nearby the apex is reduced.

Quantitative heat transfer distributions in external flows are generally presented in terms of the Stanton number St. The chordwise St distribution for Re = 1.65×10^6 and several α values is shown in Fig.4. As can be seen transition moves towards the trailing edge as α increases. This is because the laminar core becomes larger due to the axial velocity component decrease on the leeward side.

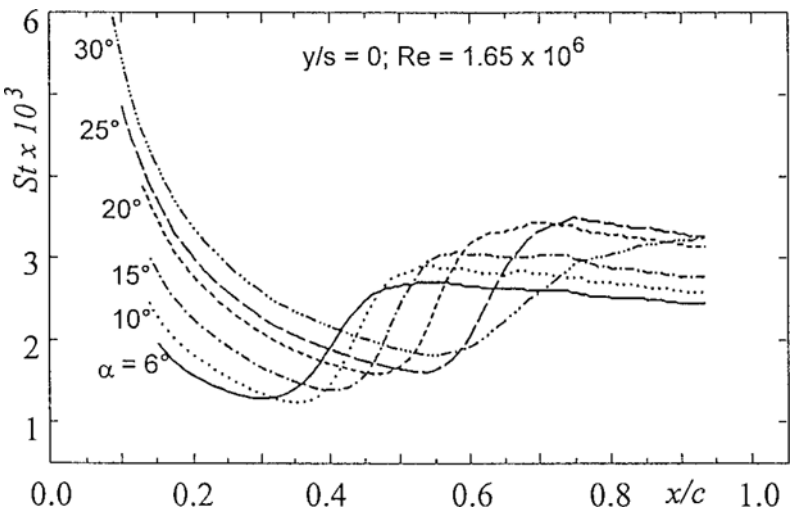

Fig. 4. Chordwise *St* profile on ℄ for various angles of attack α.

3.2. Rotating Disk

The presence of spiral vortices in the transitional regime of the three-dimensional boundary layer on a disk rotating in still air has received considerable attention (Kobayashi et al., 1980; Kohama, Y., 1984). These vortices are attached to the disk surface and therefore rotate with it.

In the present tests, the disk section consists of a 450mm OD stainless steel cup filled with a 20mm polyurethane foam on which a heating printed circuit board is glued; the rotating speed of the disk ω is varied so as to have the Reynolds number Re_ω, computed at the disk edge, in the range 86 000-690 000. Details on the experimental apparatus and procedure are reported by Cardone et al. (1997).

When the IRSR takes a two-dimensional thermal image of the disk while is rotating, the picture is of the type reported in Fig. 5 for Re_ω = 690 000. Nearby the disk center, the temperature is practically constant since the flow is laminar there; the constant heat flux boundary condition, due to the unchanging value of *h* (Cardone et al., 1997), corresponds to a constant temperature distribution. In the outer zone, the temperature decreases sharply in the transitional regime and finally more gradually in the turbulent regime. As Re_ω increases, the extension of the laminar region reduces. Obviously, the temperature map of Fig.5 is in a sense *blurred* because of the rotation of the disk. In fact, during the exposure time of the whole image, the disk makes more than 2 revolutions.

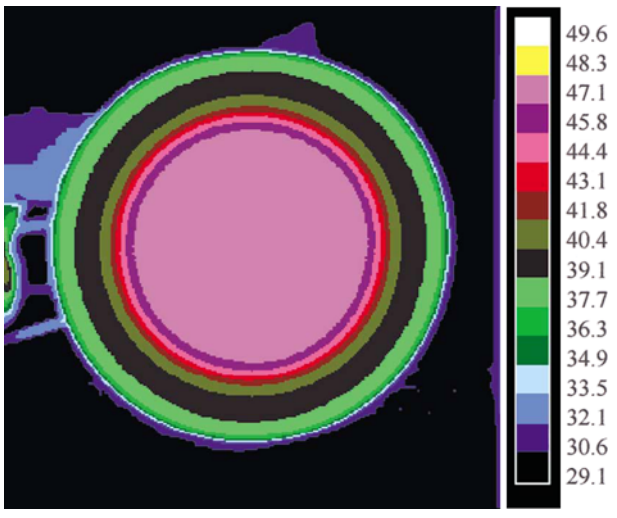

Fig. 5. Blurred wall temperature map for Re_ω = 690 000.

In order to detect the spiral vortices attached to the disk surface, the *line-scan* option of AGEMA 900 IR camera is used to take the temperature profile along one radius as a function of time at thermal steady state. Since the disk is rotating, it is possible to reconstruct the temperature map on the surface of the disk by taking into account the rotation of the latter. Such a reconstruction, which is made by superimposing about 60 000 radial profiles, is represented in Fig.6 where the spiral vortices are clearly evident. Their number and inclination with respect to the radial direction well agree with previous values reported in the literature.

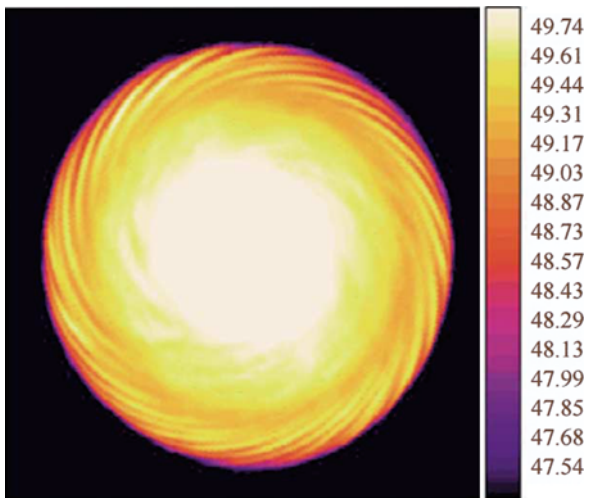

Fig. 6. Reconstructed wall temperature map for Re_∞ = 320 000.

3.3. *Jet Impingement*

The impingement of fluid jets on a solid surface has been and is still of great interest because of its several industrial applications. In the present experiments a thin constantan foil (50 μm thick) is struck by a jet directed perpendicular to it; the jet is obtained by flowing air, coming from a compressor, through a truncated cone nozzle, 50 mm long and with an exit section diameter D = 5 mm. Tests are carried out by varying the jet exit initial velocity, and therefore its Mach number and Reynolds number (based on D), and the impingement distance from the exit section of the nozzle to the target plate Z. The jet stagnation temperature T_o is kept equal to the ambient temperature and the foil is *unheated*, i.e. the adiabatic wall temperature T_{aw} over it is measured. Further details on the experimental setup are reported by Meola et al. (1996).

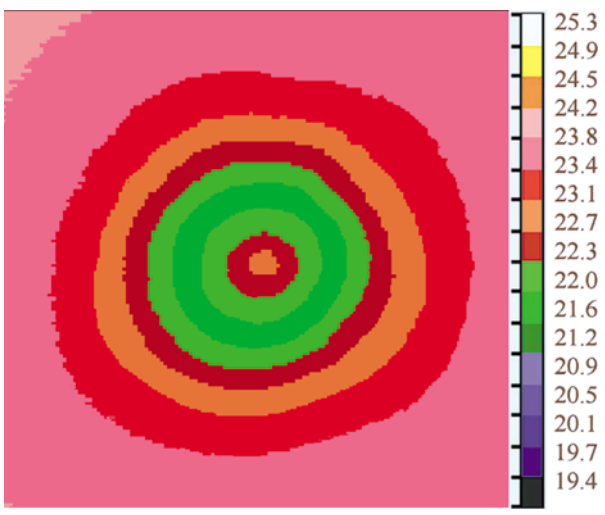

Fig. 7. Adiabatic wall temperature distribution for M = 0.4, Z/D = 4.

For very low Mach number (M<0.2) the adiabatic wall temperature T_{aw} is quite uniform over the target plate, T_{aw} being practically equal to the jet total, and/or static temperature. For Mach number increasing and Z/D < 6, as shown in Fig. 7, a local minimum appears in the shear layer, due to the presence of the vortex ring; in more details, the adiabatic wall temperature assumes a value quite equal to ambient in the jet center (stagnation point), decreases moving outward till $R/D \cong 1.6$, where it reaches the minimum value, and afterwards it goes back to the ambient value. From Fig. 7 it is possible to notice that the T_{aw} distribution is practically axisymmetric.

As the Mach number further increases, the vortex ring strengthens up to its highest magnitude and for $M \cong 0.7$ breaks up upon impact with the wall leading to entrainment of warmer ambient air. As a consequence, in the radial direction, two minima, with a maximum between them, are formed that are associated with the splitting of the primary vortex ring into two secondary vortex rings. A direct feature is that the T_{aw} distribution loses its circumferential appearance and shows azimuthal structures. The aforementioned effect is clearly evident in Fig. 8, for $Z/D = 4$ and $M = 0.81$.

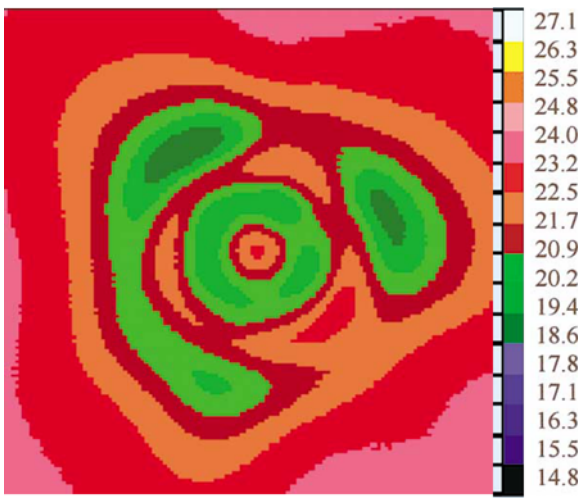

Fig. 8. Adiabatic wall temperature distribution for $M = 0.81$, $Z/D = 4$.

In the present tests both the apparatus and the experimental procedure are very simple since it is not necessary to heat the foil.

3.4. Flow Inside a 180deg Turn Static Smooth Channel

Many studies, experimental as well as numerical have been made concerning the thermal behavior of a fluid into 180deg turn channels, amongst others Chyu (1991), Lau et al. (1994); the interest is mainly justified by the industrial application for cooling turbine blades.

A two-pass channel with four different aspect ratios AR (AR = 1, 2, 3 and 5) is presently tested; the channel cross section is 80 mm (or 40, or 26.67, or 16 mm) high, 80 mm wide and 2000 mm long before the turn; the last dimension ensures a hydrodynamically fully developed flow ahead of the 180deg turn. The central partition wall between the two adjacent ducts is 16mm thick and ends with a square tip which is 80 mm distant from the short side of the channel.

Air flowing in the channel is heated from one side wall only by a printed circuit board. The heat transfer coefficient is calculated by means of Eq.(1) where $T_R = T_b$. In this case T_b is the stream bulk temperature which is evaluated by measuring the stagnation temperature at the channel entrance and by making a one-dimensional energy balance along the channel. Data is reduced in non-dimensional form in terms of the Nusselt number Nu. It has to be stressed that temperature, and consequently Nu, values very close to the side walls are not reliable since the latter, which are bonded to the printed circuit board and are not heated, tend to behave like fins.

Present data are corrected for both radiation heat transfer losses and non isotropic tangential conduction within the printed circuit board. Corrections because of the presence of natural convection from the viewed bottom surface of the heated wall are also considered. Both the Nusselt number and the Reynolds number are based on the hydraulic diameter of the channel d.

The distribution of the local Nusselt number *Nu* in the vicinity of the turn, normalized by its fully developed counterpart *Nu** (Dittus-Boelter correlation) is reported in Fig. 9 for Re_d = 60 000 and the four aspect ratios.

By moving streamwise along the heated zone of the channel *Nu/Nu** increases around the turn and downstream of it because of secondary flows. In more details, three high heat transfer regions may be recognized: the first one is located close to the end wall (in front of the partition wall towards the first outer corner) and is

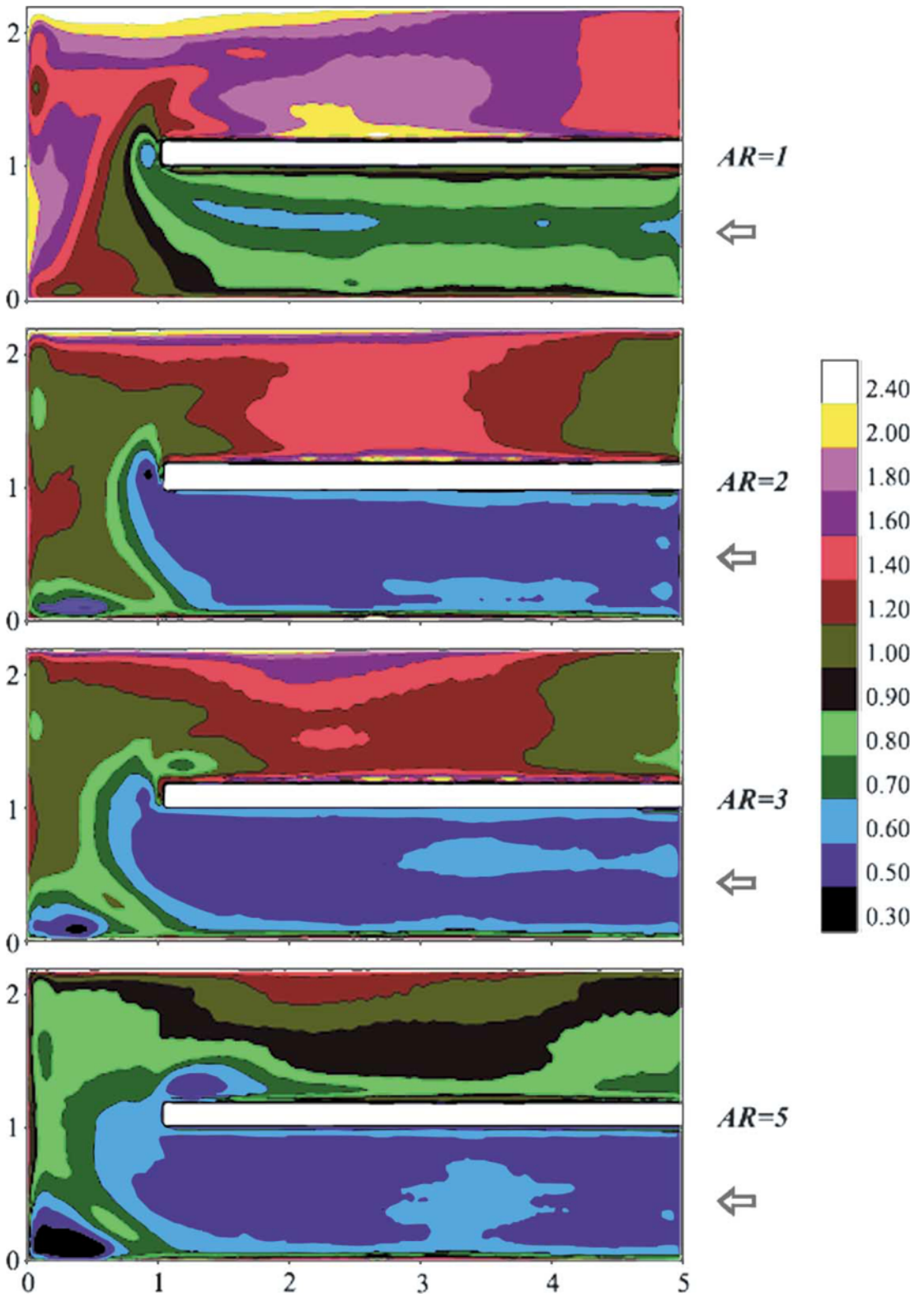

Fig. 9. Normalized Nusselt number maps for the four different aspect ratios (Re_d = 60 000).

caused by the jet coming from the first duct which impinges on this wall; the second one is located downstream of the second corner of the outer wall and is due to the *jet* effect of the flow through the bend; the third one is located at about the half part of the partition wall, downstream of the second inner corner, where the flow *rebounding* from the outer wall, impinges before exhaust. The second zone attains *Nu/Nu** values greater than the other two high heat transfer zones. Two low heat transfer zones are also observed, one just before the first corner of the outer wall and the other one in the neighbourhood of the tip of the partition wall; these zones make evidence of the existence of recirculation bubbles. Another small zone, exhibiting a low heat transfer coefficient, is positioned nearby the end wall, practically across the exhaust duct axis.

As the aspect ratio *AR* is increased from 1 to 5, the average heat transfer coefficient decreases and the heat transfer peaks tend to progressively reduce; the first recirculation bubble (in the first outer corner) strengthens; the second recirculation bubble, which is initially located over the tip for *AR* = 1, slips downstream and, for *AR* = 5, is attached to the partition wall just downstream of the second inner corner.

3.5. 180deg Turn Static Channel with Ribs

To enhance heat transfer inside channels like those presented in the previous section, regular geometric roughness elements (ribs), which act as turbulence promoters, are placed at their walls.

The data herein presented refer to tests performed in the channel, described in the previous section, with *AR* = 1 and with aluminum ribs of square cross section (8×8 mm^2) placed at 80mm pitch along the channel axis and at two different angles γ with respect to the flow direction. The main effect of such ribs is to enhance the convective heat transfer coefficient; from this point of view it is found that, the configuration with ribs positioned at an angle of inclination $\gamma = 30^\circ$ is preferable to that with ribs perpendicularly ($\gamma = 90^\circ$) positioned with respect to the flow direction. It is also worth noting that the first configuration entails lower flow resistance.

The normalized Nusselt number distribution in the vicinity of the turn is shown in Fig.10 for Re_d = 30 000 and the two γ values. High heat transfer values are always present over the *ribs*. The thermal reattachment lines, downstream of the perpendicular ribs are clearly evident as well as the occurring of low heat transfer zones in the downstream part of the space between two adjacent inclined ribs. In the U turn region for the perpendicular rib case, a low heat transfer zone is present downstream of the last rib of the inlet channel and attached to the side wall

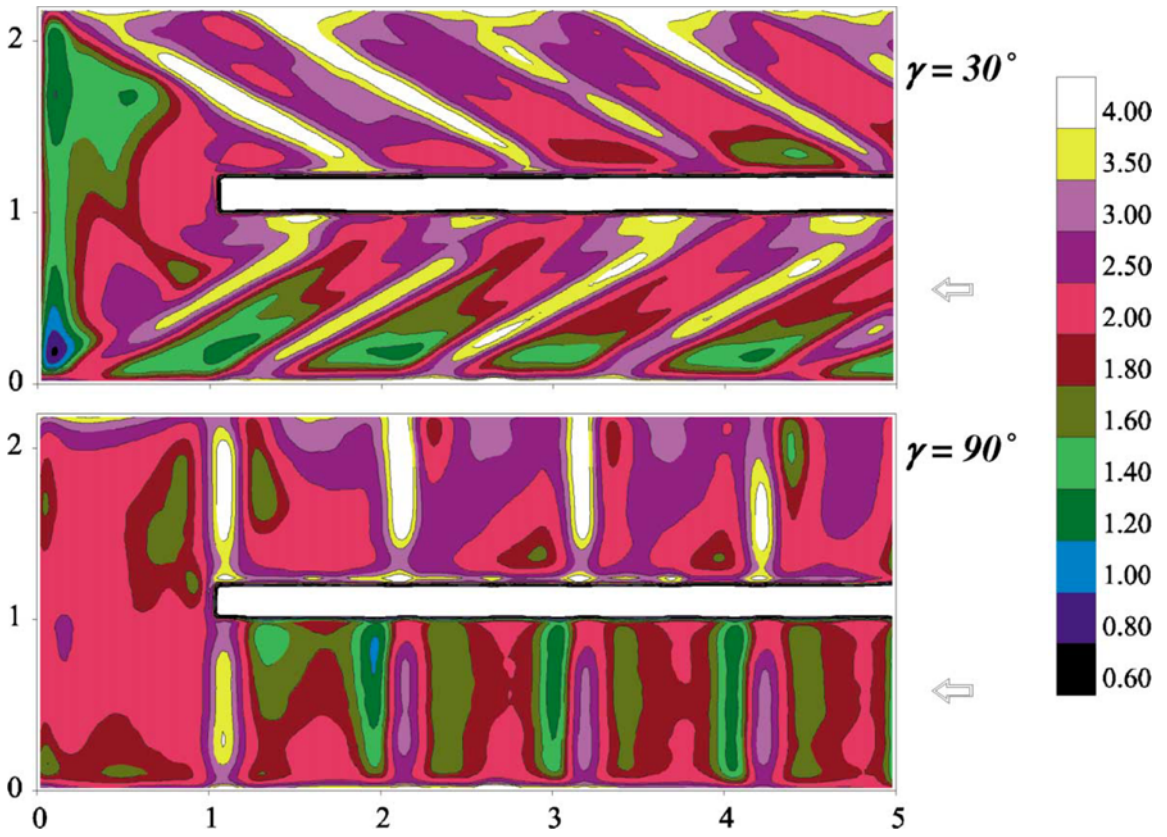

Fig. 10. Normalized Nusselt number maps for the ribbed channel (Re_d = 30 000).

while on the other side a high heat transfer zone is still present (as in the non ribbed case) even further downstream. For the inclined rib case, two low heat transfer zones are present at the end wall nearby the two outer corners. It is also possible to notice the effects of the secondary flows induced by the ribs inclination, e.g., nearby the partition wall, the higher *Nu* value in the inlet channel and the lower one in the outlet channel.

3.6. Flow Inside a 180deg Turn Rotating Smooth Channel

The rotation of a turbine blade gives rise to Coriolis and buoyancy forces that may completely change the distribution of the local heat transfer coefficient described in Section 3.4.

For radially outward flow the Coriolis force produces a secondary flow in the plane perpendicular to the direction of the moving fluid, which pushes the particle in the center of the channel towards the trailing surface. With respect to the non-rotating case, these secondary cells enhance the heat transfer in the vicinity of the trailing wall and reduce it at the leading surface. When the flow is reversed, i.e. radially inward flow, one has only to change the role played by the leading surface with that of the trailing one and vice versa. Furthermore, the wall heating causes a temperature difference between the core and the wall regions so that the strong centripetal acceleration due to rotation gives rise to a buoyant effect which magnifies the influence of the Coriolis force in the radially outward flow and reduces it in the opposite case.

In the present tests the rotating arm includes a two pass square channel, 22 mm in side and 330 mm in length which is mounted on a shaft whose angular speed may be varied in a continuos way, in the range 0-2000 rpm. Since the channel is rotating during the tests, it is not possible to take its whole thermal picture in one shot; it is then necessary to make use of the line scan facility of the AGEMA 900, in order to take advantage of the much higher acquisition frequency of a line (2550 Hz instead of 15 Hz for the full frame), and to reconstruct the whole image by joining together the several lines acquired at steady thermal state. Details of the experimental apparatus and procedure are reported by Astarita et al. (1997).

The investigated physical phenomenon is mainly governed by the Reynolds number Re_d, the rotation number *Ro* (which is also the reciprocal of the Rossby number) and the buoyancy parameter Bu. In Fig.11 the temperature maps for the static and the *rotating* cases are presented. A comparison between the first image of Fig.9 and the first and the third ones of Fig.11 shows some differences, amongst others the lack of the very low and very high heat transfer zones in the second ones. This may be ascribed to several reasons. First of all, the relative thickness of the partition wall, which as compared to the channel side, is double in the second case and softens rotation around the turn. Then, the Reynolds number in the map of Fig.11 is much lower than that in the map of Fig.9. Finally, the spatial resolution in the smaller channel is lower because of its size.

In Fig.11 the images for the static channel (*Ro*=0) are shown for two different inlet temperatures (one for the trailing and one for the leading wall which are actually the same situation) so as to have an easier comparison with the rotating channel walls which, correspondingly, have the same inlet temperatures. By recalling Eq.(1) and assuming that T_b is equal in the two cases, which is true if the two radiation losses are practically equal, the maps seem to agree with the assertions previously made. Indeed, at the trailing wall the lower values of temperature reached in the rotating channel (with respect to the non-rotating one) for the radially outward flow is a witness to a higher heat transfer coefficient, while the reverse is true for the inward flow. As far as the leading wall is concerned, the opposite behavior is evidenced, i.e., for the rotating channel, the higher temperature values in the outward flow confirm a lower heat transfer coefficient while, to a lower extent, the value of *h* is higher in the inward flow. This is because of the presence of the buoyant effect.

4. Conclusions

Some fluid flow configurations have been analyzed by means of infrared thermography applied to the *heated-thin-foil* technique and it has been proved that IRSR is able to detect, through temperature distributions, the flow dynamic and related secondary phenomena.

The central region of the delta wing surface is characterized by an almost two-dimensional flow; moving from the apex in streamwise direction along the root chord, a gradual increase in temperature is first observed, followed by a sharp drop, due to the development of the laminar boundary-layer and to transition. By moving from the leading edge, along the wing span, towards the root chord the temperature takes a minimum followed by an increase and a successive decrease, due to the presence of primary and secondary vortices. An increase of the angle of attack widens the laminar core and delays transition. After transition, the outward displacement of the secondary separation line is clearly identified. When the flow becomes turbulent, also the primary *thermal* reattachment line

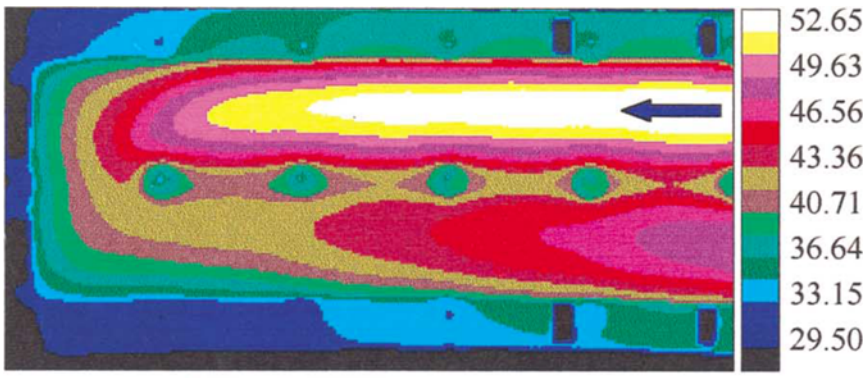

Fig. 11. Wall temperature maps for the static (Ro = 0) and the rotating (Ro = 0.3) channels.

moves towards the leading edge of the wing.

The presence of spiral vortices in the transitional regime of the flow of a disk rotating in still air has been detected by means of the line-scan option of the IRSR and by reconstructing the temperature distribution over the disk surface. The number and inclination of the vortices well agree with previous data.

In an impinging jet, at the critical Mach number (0.7), the vortex ring breaks up giving rise to the formation of azimuthal structures. This event has been detected by merely measuring the adiabatic wall temperature of the impinged surface.

In the 180deg turn, three high heat transfer regions may be recognized along the streamwise direction of the channel: the first one is located very close to the end wall in front of the tip towards the first outer corner; the second one is located downstream of the second corner of the outer wall and the third one is located at about the half part of the inner wall, far away from the second inner corner where the flow impinges before exhaust. Two low heat transfer zones which evidence the presence of recirculation bubbles are also present, one in the vicinity of the first corner of the outer wall and the other one in the neighbourhood of the tip of the partition wall. As the aspect ratio increases, the high heat transfer zones tend to weaken and to move downstream, the first recirculation bubble strengthens and the second one slips downstream of the tip of the partition wall.

The presence of ribs along the channel enhances heat transfer. The configuration with inclined ribs is preferable to that with ribs perpendicular to the channel flow also because of their lower flow resistance.

In rotating channels, as the rotational speed increases, at the trailing wall, the inward flow attains higher average heat transfer coefficients; the opposite happens to the outward flow; instead, at the leading wall, the heat transfer slightly decreases in the inward channel and increases in the outward one. It has to be noted that in the inversion zone, the heat transfer values relative to the leading edge are higher than those relative to the trailing one.

References

Astarita, T., Cardone, G. and Carlomagno, G. M., IR Heat Transfer Measurements in a Rotating Channel, to be published on Proceedings of the Seminar on Quantitative Infrared Thermography (QIRT 96), Balageas D., Busse G. and Carlomagno G.M. eds. (1997).

Balageas, D. L., Boscher, D. M., Déom, A. A., Fournier, J. and Gardette, G., Measurement of Convective Heat Transfer Coefficients in Wind Tunnels using Passive and Stimulated Infrared Thermography, Rech. Aerosp., 1991-4, (1991), 51-72.

Bynum, D. S., Hube, F. K., Key, C. M. and Diek, P. M., Measurement and Mapping of Aerodynamic Heating with an Infrared Camera, AEDC Rept. TR-76-54, (1976), 1-33.

Cardone, G., Astarita, T. and Carlomagno, G. M., Infrared Thermography to Measure Local Heat Transfer Coefficients on a Disk Rotating in Still Air, Proceedings of the Workshop Advanced Infrared Technology and Applications, (1996), 143-153, Baccini & Baldi, Firenze.

Cardone, G., Astarita, T. and Carlomagno, G. M., Heat Transfer Measurements on a Rotating Disk, Int. J. Rotating Machinery, 3, (1997), 1-9.

Carlomagno, G. M. and de Luca L., Handbook of Flow Visualization, (ed. W.J. Yang) chap. 32, (1989), 531-553, Hemisphere.

Carlomagno, G. M., de Luca, L. and Alziary de Roquefort, T., Mapping and Measurement of Aerodynamic Heating and Surface Flow Visualization by means of IR Thermography, in Multiphase Flow and Heat Transfer, (Eds. Chen et al.), 2, (1991), 1316-1324, Hemisphere.

Carlomagno G. M., Heat Transfer Measurements by means of Infrared Thermography, in Measurement Techniques, von Karman Institute for Fluid Mechanics Lect. Series 1993-05, (1993), 1-114, Rhode-Saint-Genese.

Carlomagno, G. M., Surface Flow Visualization of a Backward-Facing Step Flow, in Y. Nakayama and Y. Tanida (eds.) Atlas of Visualization II, chap.7, (1996), CRC press, New York.

Carlomagno, G. M., Thermo-fluid-Dynamic Applications of Quantitative Infrared Thermography, Proceedings of the 1st Pacific Symposium on Flow Visualization and Image Processing 1, (1997), 35-45, Honolulu.

Chyu, M. K., Regional Heat Transfer in Two-Pass and Three-Pass Passages with 180-deg Sharp Turns, ASME J. of Heat Transfer, 113, (1991), 63-70.

De Luca, L., Carlomagno, G. M. and Buresti, G., Boundary Layer Diagnostics by means of an Infrared Scanning Radiometer, Experiments in Fluids, 9, (1990), 121-128.

De Luca, L., Cardone, G., Carlomagno, G. M., Aymer de la Chevalerie, D. and Alziary de Roquefort, T., Flow Visualization and Heat Transfer Measurement in a Hypersonic Wind Tunnel, Experimental Heat Transfer, 5, (1992), 65-78.

Henckels, A., Maurer, F., Olivier, H. and Grönig, H., Fast Temperature Measurement by Infrared Line Scanning in a Hypersonic Shock Tunnel, Experiments in Fluids, 9, (1990), 298-300.

Lau, S.C., Russell, L. M., Thurman, D.R. and Hippensteele, S. A., Channels with Liquid Chrystals, Proc. V Int. Symp. On Transport Phenomena and Dynamics of Rotating Machinery, A, (1994), 411-423, Kaanaply, Hawaii.

Lee, M. and Ho, C.M., Lift Force of Delta Wings, Applied Mechanics Review, 43,n.9 (1990).

Kobayashi, R., Kohama, Y. and Takamadate, Ch., Spiral Vortices in Boundary Layer Transition Regime on a Rotating Disk, Acta Mech., 35, (1980), 71-82.

Kohama, Y., Study on Boundary Layer Transition of a Rotating Disk, Acta Mech., 50, (1984), 193-199.

Meola, C., de Luca, L. and Carlomagno, G. M., Influence of Shear Layer Dynamics on Impingement Heat Transfer, Experimental Thermal and Fluid Science, 13, (1996), 29-37.

Nelson, R. C., Unsteady Aerodynamics of Slender Wings, AGARD Rept 776, (1991).

Simeonides, G., D. Van Lierde, P., Van der Stichele S., Capriotti and Wendt J. F., Infrared Thermography in Blowdown and Intermittent Hypersonic Facilities, AIAA Paper 89-0042 (1989).